

Supporting Information

Weichsel et al. 10.1073/pnas.0913730107

SI Text

Linear Stability Analysis of the Reduced Rate Equation Approach. In the rate equation approach, the number of filament ends in the branching region with angles between θ and $\theta + d\theta$ is given by $N(\theta, t)d\theta$. By integrating this equation stepwise over finite-sized angle bins, we obtain a finite number of coupled ordinary differential equations describing the temporal behavior of the filament number in every angle bin:

$$N_{\bar{\theta}} = \int_{\bar{\theta}-\Delta\theta/2}^{\bar{\theta}+\Delta\theta/2} N(\theta', t) d\theta' \quad [\text{S1}]$$

with mean angle $\bar{\theta}$ and width $\Delta\theta$. For a numerical solution, we typically choose 360 angle bins. For analytical progress, we reduce the number of equations by choosing a large bin with a size of $\Delta\theta = 35^\circ$, that is, half of the Arp2/3 branching angle. In addition we assume that branching is restricted to pairs of angle bins with a relative angle difference of 70° , that the rate according to which filaments grow out of the branching region is given by the rate for the mean angle of the corresponding bin $k_{\text{gr}}(\bar{\theta})$, and that the branching of filaments with $|\theta| > 87.5^\circ$ can be neglected as they grow out of the branching region sufficiently quickly. We then arrive at a system of five differential equations:

$$\frac{\partial N_{-70^\circ}}{\partial t} = \frac{1}{2} \hat{k}_b N_{0^\circ} - (k_c + k_{\text{gr}}(70^\circ)) N_{-70^\circ} \quad [\text{S2}]$$

$$\frac{\partial N_{-35^\circ}}{\partial t} = \frac{1}{2} \hat{k}_b N_{+35^\circ} - (k_c + k_{\text{gr}}(35^\circ)) N_{-35^\circ} \quad [\text{S3}]$$

$$\frac{\partial N_{0^\circ}}{\partial t} = \frac{1}{2} \hat{k}_b (N_{-70^\circ} + N_{+70^\circ}) - k_c N_{0^\circ} \quad [\text{S4}]$$

$$\frac{\partial N_{+35^\circ}}{\partial t} = \frac{1}{2} \hat{k}_b N_{-35^\circ} - (k_c + k_{\text{gr}}(35^\circ)) N_{+35^\circ} \quad [\text{S5}]$$

$$\frac{\partial N_{+70^\circ}}{\partial t} = \frac{1}{2} \hat{k}_b N_{0^\circ} - (k_c + k_{\text{gr}}(70^\circ)) N_{+70^\circ}, \quad [\text{S6}]$$

with

$$\hat{k}_b = \frac{k_b}{\mathcal{W}_{\text{tot}}} = \frac{k_b}{N_{-70^\circ} + N_{-35^\circ} + N_{0^\circ} + N_{+35^\circ} + N_{+70^\circ}}.$$

Due to the symmetry around 0° , only three of these equations are independent.

To identify and analyze the stationary states of Eqs. S2–S6, we are solving $\partial N_{\bar{\theta}}/\partial t = 0$ for all $\bar{\theta}$. If we take into account only the physically meaningful subspace of nonnegative filament numbers, two steady-state solutions emerge. The first solution,

$$\begin{aligned} N_{-70^\circ}^{\text{ss35}} &= 0, & N_{-35^\circ}^{\text{ss35}} &= k_b \frac{1}{4(k_c + k_{\text{gr}}(35^\circ))}, & N_{0^\circ}^{\text{ss35}} &= 0, \\ N_{+35^\circ}^{\text{ss35}} &= k_b \frac{1}{4(k_c + k_{\text{gr}}(35^\circ))}, & N_{+70^\circ}^{\text{ss35}} &= 0, \end{aligned} \quad [\text{S7}]$$

represents a dominant $\pm 35^\circ$ orientation distribution in the steady state (ss35) while the second solution,

$$\begin{aligned} N_{-70^\circ}^{\text{ss70}} &= k_b \frac{k_c + k_{\text{gr}}(70^\circ) - \sqrt{2k_c(k_c + k_{\text{gr}}(70^\circ))}}{2(k_{\text{gr}}^2(70^\circ) - k_c^2)}, & N_{-35^\circ}^{\text{ss70}} &= 0, \\ N_{0^\circ}^{\text{ss70}} &= k_b \frac{1 - \sqrt{\frac{k_c + k_{\text{gr}}(70^\circ)}{2k_c}}}{k_c - k_{\text{gr}}(70^\circ)}, & N_{+35^\circ}^{\text{ss70}} &= 0, \\ N_{+70^\circ}^{\text{ss70}} &= k_b \frac{k_c + k_{\text{gr}}(70^\circ) - \sqrt{2k_c(k_c + k_{\text{gr}}(70^\circ))}}{2(k_{\text{gr}}^2(70^\circ) - k_c^2)}, \end{aligned} \quad [\text{S8}]$$

corresponds to the competing $+70/0/-70^\circ$ pattern (ss70).

In order to investigate how the stability of these fixed points depends on model parameters, we use linear stability analysis. For this purpose, the eigenvalues λ_i of the Jacobi matrix of the nonlinear system (Eqs. S2–S6) at the positions of the fixed points N^{ss35} (solution S7) and N^{ss70} (solution S8) have to be calculated. Starting with ss35, the eigenvalues of the Jacobi matrix read

$$\lambda_1^{\text{ss35}} = -(k_c + k_{\text{gr}}(35^\circ)) \quad [\text{S9}]$$

$$\lambda_2^{\text{ss35}} = -2(k_c + k_{\text{gr}}(35^\circ)) \quad [\text{S10}]$$

$$\lambda_3^{\text{ss35}} = -(k_c + k_{\text{gr}}(70^\circ)) \quad [\text{S11}]$$

$$\lambda_4^{\text{ss35}} = -\frac{1}{2} (2k_c + k_{\text{gr}}(70^\circ) + \sqrt{8(k_c + k_{\text{gr}}(35^\circ))^2 + k_{\text{gr}}^2(70^\circ)}) \quad [\text{S12}]$$

$$\lambda_5^{\text{ss35}} = -\frac{1}{2} (2k_c + k_{\text{gr}}(70^\circ) - \sqrt{8(k_c + k_{\text{gr}}(35^\circ))^2 + k_{\text{gr}}^2(70^\circ)}). \quad [\text{S13}]$$

Note that the branching rate k_b does not appear in the eigenvalues and therefore has no influence on the stability of the steady state. This means we have to determine for which sets of parameters k_c , $k_{\text{gr}}(35^\circ)$, and $k_{\text{gr}}(70^\circ)$ all eigenvalues are strictly negative, because for these sets the fixed point N^{ss35} is asymptotically stable. However, the two parameters $k_{\text{gr}}(35^\circ)$ and $k_{\text{gr}}(70^\circ)$ are not independent, but rather both of them are determined by the bulk velocity of the network v_{nw} as given in Eq. 3 of the main text. If we omit the ill-defined cases $k_c = k_{\text{gr}}(35^\circ) = 0$ and $k_c = k_{\text{gr}}(70^\circ) = 0$, the first four eigenvalues $\lambda_1^{\text{ss35}} - \lambda_4^{\text{ss35}}$ are strictly negative for all possible (nonnegative) values for the parameters. The last eigenvalue λ_5^{ss35} , however, changes its sign when the relation

$$k_{\text{gr}}(70^\circ) = \frac{k_c^2 + 4k_c k_{\text{gr}}(35^\circ) + 2k_{\text{gr}}^2(35^\circ)}{k_c} \quad [\text{S14}]$$

is satisfied.

Although the expressions for some of the eigenvalues of the ss70 solution are rather complicated, it can be shown that in this case also only one eigenvalue

$$\lambda_5^{\text{ss70}} = -k_c - k_{\text{gr}}(35^\circ) + \sqrt{\frac{k_c(k_c + k_{\text{gr}}(70^\circ))}{2}} \quad [\text{S15}]$$

changes its sign, whereas all the others are strictly negative in the parameter range mentioned before. The sign of $\lambda_5^{\text{ss}70}$ changes under the same condition as we have found before for $\lambda_5^{\text{ss}35}$ (Eq. S14). However, both eigenvalues $\lambda_5^{\text{ss}35}$ and $\lambda_5^{\text{ss}70}$ hold opposite signs whenever they do not vanish. Therefore we can conclude that for the whole parameter range (apart from the subset where Eq. S14 is exactly satisfied), either the ss35 steady state is asymptotically stable and the ss70 solution is a saddle, or vice versa.

Next we analyze for which bulk network velocities v_{nw} Eq. S14 is fulfilled. If we start at small v_{nw} such that the critical angle is $\theta_c \geq 70^\circ$ and only filaments with a larger orientation angle than θ_c are growing out of the branching region, we get from Eq. 3 of the main text $k_{\text{gr}}(70^\circ) = k_{\text{gr}}(35^\circ) = 0$ and Eq. S14 is never fulfilled (for $k_c > 0$). For increasing network speed, $35^\circ \leq \theta_c < 70^\circ$ (i.e., $k_{\text{gr}}(70^\circ) > 0 \wedge k_{\text{gr}}(35^\circ) = 0$), we obtain a single solution for v_{nw} that satisfies Eq. S14,

$$v_{\text{nw}} = \frac{1}{2}d_{\text{br}}k_c + v_{\text{fil}} \cos(70^\circ), \quad \text{for } 35^\circ \leq \theta_c < 70^\circ. \quad [\text{S16}]$$

Once the network velocity has reached the value where the critical angle $\theta_c < 35^\circ$ (i.e., $k_{\text{gr}}(70^\circ) > k_{\text{gr}}(35^\circ) > 0$), two solutions emerge:

$$v_{\text{nw}1,2} = \frac{1}{8}(-3k_c d_{\text{br}} + 8v_{\text{fil}} \cos(35^\circ)) \pm \frac{1}{8} \sqrt{k_c d_{\text{br}}(k_c d_{\text{br}} + 16v_{\text{fil}} \cos(35^\circ) - 16v_{\text{fil}} \cos(70^\circ)),}$$

for $\theta_c < 35^\circ$. [S17]

Due to the restrictions on the critical angle, solution [S16] is valid for network bulk velocities $v_{\text{fil}} \cos(35^\circ) \geq v_{\text{nw}} > v_{\text{fil}} \cos(70^\circ)$, whereas solution [S17] holds in the domain $v_{\text{nw}} > v_{\text{fil}} \cos(35^\circ)$. This restriction is never fulfilled by the negative square root in Eq. S17, and so we can neglect this solution in the following. A phase diagram showing the separate regions in which either ss35 is asymptotically stable and ss70 is a saddle or vice versa is given in Fig. 24 of the main text. There the constants were chosen such that filament barbed ends grow with a velocity v_{fil} of one actin monomer increment δ_{fil} per unit time step and the width of the branching region d_{br} equals $2\delta_{\text{fil}}$.

So far, we have seen that the system, starting in close proximity of the stable fixed point, will eventually end up in this state. We now have to also treat the saddle point. Although this point is repelling in a single dimension (given by the eigenvector of the positive eigenvalue), there is also a four-dimensional subspace (the remaining four eigenvectors) of initial conditions attracted to this state in its neighborhood. In the following it will be specified which initial conditions exactly are still converging to the saddle.

Let us assume we are in the parameter range in which the ss35 is a node while the ss70 solution is a saddle point. If we evaluate the subspace spanned by the four eigenvectors $\vec{v}_i^{\text{ss}70}$ with negative eigenvalues at the saddle, they have the form

$$\vec{v}_1^{\text{ss}70} = \begin{pmatrix} 1 \\ 0 \\ 0 \\ 0 \\ -1 \end{pmatrix}, \quad \vec{v}_2^{\text{ss}70} = \begin{pmatrix} 0 \\ 1 \\ 0 \\ -1 \\ 0 \end{pmatrix}, \quad \vec{v}_3^{\text{ss}70} = \begin{pmatrix} 1 \\ 0 \\ 0 \\ 0 \\ 1 \end{pmatrix},$$

$$\vec{v}_4^{\text{ss}70} = \begin{pmatrix} 1 \\ 0 \\ b \\ 0 \\ 1 \end{pmatrix}, \quad [\text{S18}]$$

where a and b are constants depending on the parameters. Here we can see that the eigenvectors $\vec{v}_1^{\text{ss}70}$, $\vec{v}_3^{\text{ss}70}$, and $\vec{v}_4^{\text{ss}70}$ span the three-dimensional subspace where the $N_{\pm 35^\circ}$ fiber population vanishes. As the two different orientation distributions are not coupled via branching in this model, this is a trivial case. From initial conditions where there are no fibers in the $N_{\pm 35^\circ}$ orientation bins, this steady state can never be reached. The remaining eigenvector $\vec{v}_2^{\text{ss}70}$ however spans a subspace only featuring non-physical (negative) fiber numbers in exactly one bin. Therefore we can conclude that initial conditions of positive fiber numbers in all bins will in general not approach this saddle point in the system.

A similar reasoning applies for parameters for which the ss35 fixed point is unstable. Again we can write down the eigenvectors of the negative eigenvalues, i.e., the subspace that is attracted to the saddle in its vicinity

$$\vec{v}_1^{\text{ss}35} = \begin{pmatrix} 0 \\ 1 \\ 0 \\ 1 \\ 0 \end{pmatrix}, \quad \vec{v}_2^{\text{ss}35} = \begin{pmatrix} 0 \\ -1 \\ 0 \\ 1 \\ 0 \end{pmatrix}, \quad \vec{v}_3^{\text{ss}35} = \begin{pmatrix} -1 \\ 0 \\ 0 \\ 0 \\ 1 \end{pmatrix},$$

$$\vec{v}_4^{\text{ss}35} = \begin{pmatrix} 1 \\ a \\ b \\ a \\ 1 \end{pmatrix}, \quad [\text{S19}]$$

where a is again some constant depending on the parameters, and b is given by

$$b = \frac{k_{\text{gr}}(70^\circ) - \sqrt{8(k_c + k_{\text{gr}}(35^\circ))^2 + k_{\text{gr}}(70^\circ)^2}}{2(k_c + k_{\text{gr}}(35^\circ))}. \quad [\text{S20}]$$

As $b < 0$ for all relevant sets of parameters, we can conclude again that the vectors $\vec{v}_1^{\text{ss}35}$ and $\vec{v}_2^{\text{ss}35}$ span the trivial subspace where no fibers are in the $N_{\pm 70^\circ}$ and N_{0° orientation bins and the remaining vectors $\vec{v}_3^{\text{ss}35}$ and $\vec{v}_4^{\text{ss}35}$ span a subspace in which at least one fiber number is negative. Therefore here again all physically meaningful conditions in the vicinity of the saddle point will be repelled.

In the phase diagram shown in Fig. 24 of the main article, the ± 35 pattern vanishes at large capping rate. This feature of the reduced rate equation model follows from the assumption that filaments with an orientation larger than 87.5° do not branch. As the capping rate increases, the angle-dependent outgrowth term favoring persistence of filaments with small angles becomes less important and the $-70/0/70$ pattern is favored because it involves more angle bins. As the full rate equation model and the stochastic network growth model do not share this assumption, they do not predict the elimination of the ± 35 pattern for large capping rate.

Analysis of the Order Parameter for Different Branching and Capping Rates. Fig. S14 shows the evolution of the order parameter

$$\mathcal{O} = \frac{N_{0^\circ} - N_{35^\circ}}{N_{0^\circ} + N_{35^\circ}} = [-1, +1] \quad [\text{S21}]$$

for different values of the branching and capping rates as obtained from the numerical solution of the model equations with 360 angle bins and for quasistationary changes in network velocity

v_{nw} . The three curves for constant capping rate $k_c = 0.05$ but different values for the branching rate k_b , collapse, indicating that the order parameter is independent of the branching rate, as predicted from analytical stability analysis of the simplified model in section *Linear Stability Analysis of the Reduced Rate Equation Approach* of this SI. However, when the capping rate k_c is increased over three orders of magnitude, the clear distinction between the two different phases vanishes. In Fig. S1B, the two maximum values of the order parameter for the fast and slow growth phases as well as the minimum value for the medium growth phase are given for increasing capping rate. The absolute magnitude of these peak values is rapidly decreasing until the different orientation patterns can not be sufficiently discriminated anymore. This justifies a posteriori our choice of a small capping rate $k_c = 0.05$ per unit time for the simulations presented in the main text. If this value was significantly larger, one could not observe the characteristic orientation distributions found in electron micrographs of the leading edge of mobile cells (1–3).

Sensitivity of the Force–Velocity Relation to Parameter Variation. In the main text, the force–velocity relation is given as the numerical solution of the coupled Eqs. 1, 5, and 7 in Fig. 3A for the following choice of model parameters: capping rate $k_c = 0.05$ per filament and per unit time, branching rate $k_b = 20$ per unit time, and standard deviation $\sigma = 5^\circ$ of the branching angle distribution. In the following, we will analyze how sensitive the calculated force–velocity relation is to variations in these key parameters.

As discussed in the main text, a change in the branching rate has no influence on the relative filament number per angle in the network. Therefore this parameter does not alter the characteristics of the force–velocity relationship (apart from a rescaling of the total force, as the total number of filaments carrying force does change). In Fig. S2, results are shown for different values of k_c and σ . Additionally, two different values for the maximum angle θ_{fil}^{max} up to which filaments are able to carry the maximum force $f_{fil}^{max} = 1$ were assumed in the calculations. According to these results, the hysteresis cycle at the transition from fast to medium growth phase as well as the relatively flat curve during the transition from medium to slow growth phase is conserved over a wide range of parameters. However, for large values of the standard deviation of the branching angle σ , the capping rate k_c , and the angle θ_{fil}^{max} , the hysteresis cycle vanishes. This behavior can be understood as the large standard deviation as well as a large capping rate diminishes the difference in the filament orientation distribution of the two observed patterns (compare section *Analysis of the Order Parameter for Different Branching and Capping Rates* in this SI). Additionally, a larger θ_{fil}^{max} reduces the difference in load the two networks are able to carry. However, a marked difference in the ability to carry load between the two competing orientation patterns is the essential requirement for the two prominent features of the force–velocity relation, namely, the hysteresis cycle and the force-insensitive regime.

An additional feature that can be observed in Fig. S2 is that the force–velocity curves for different σ cross at a similar value of force. There exists a simple explanation for this feature: The crossing is always close to the velocity at which the transition from medium to slow growth phase takes place. For $\sigma \geq 5^\circ$, the filament orientation distribution at this velocity is approximately constant in between $-\theta_{max}$ and $+\theta_{max}$, i.e., for all filament angles that contribute in pushing the load. Therefore, an approximately equal force can be carried by the networks in this situation. For $\sigma = 2^\circ$, the velocity as a function of force is a flat curve anyway.

Force–Velocity Relation for a Network Elongating as a Brownian Ratchet. In the main text, we assumed a hypothetical protrusion efficiency of the network which differentiates the two orientation patterns sufficiently strongly to result in hysteresis effects. For comparison, here we also show the results of the force–velocity

curve under the assumption that each filament of the network elongates as a Brownian ratchet (4, 5). In this model, each filament grows according to its angle θ and the individual force it carries $f_{fil}(\theta)$ with a velocity

$$v_{fil}^\perp(\theta) = v_{fil} \cos(\theta) \exp\left(-\frac{f_{fil}(\theta)\delta_{fil} \cos(\theta)}{k_B T}\right) \quad [S22]$$

perpendicular to the leading edge. In the stationary state, the system will share the external force between the filaments in such a way that all filaments that carry load ($\theta \leq \theta_{max}$) grow with the same velocity v_{fil}^\perp and all others grow slower,

$$v_{fil}^\perp(\theta \leq \theta_{max}) = v_{fil} \cos(\theta_{max}). \quad [S23]$$

For a given force, this velocity also defines the bulk network velocity $v_{nw} = v_{fil}^\perp(\theta \leq \theta_{max})$. Hence, in the stationary state, the external force will be distributed over different filament orientations as

$$f_{fil}(\theta) = \frac{k_B T}{\delta_{fil} \cos(\theta)} \ln\left(\frac{\cos(\theta)}{\cos(\theta_{max})}\right). \quad [S24]$$

When the force on the network is increased, so will θ_{max} such that the force is redistributed and the network will continue to grow at a slower pace. By iterating Eq. S24 in combination with the network orientation from Eq. 1 of the main text, the corresponding force–velocity relation is obtained. In this simulation again the force was changed quasistationary like in the main text. That means that, after every small change in force, the system had enough time to approach a stationary state. For numerical stability, the stall force of the network was assumed to be located at the point at which all filaments in the network with an orientation $\theta \leq 89^\circ$ were not able to carry the external load anymore.

Fig. S3 shows the resulting force–velocity curve. As expected, the dependence shows a convex decrease over the whole force range. In this scenario, no significant hysteresis effects could be observed at any of the two filament orientation transitions. Hence the protrusion efficiency obtained by assuming a Brownian-ratchet mechanism does not sufficiently differentiate between the two different filament patterns. The protrusion force for proximal network growth velocities above and below each of the two transitions is weakly but monotonically increasing for decreasing network velocity. Therefore, hysteresis cycles do not emerge and the model can not explain the experimentally observed anomalies (7, 8).

Physical Values of the Model Parameters. There are three different rates which can be used to scale time: branching rate k_b , capping rate k_c , and growth rate v_{fil}/δ_{fil} . Here we choose the last one. The basic length scale of actin growth is $\delta_{fil} = 2.7$ nm. A typical filament growth velocity at close to optimal conditions is $1 \mu\text{m/s}$. Then the growth rate $370 \delta_{fil}$ per second. Therefore the branching rate $k_b = 20$ used in the simulations corresponds to $k_b = 7,410$ branching events per second in the simulated region of the network. The used capping rate $k_c = 0.05$ corresponds to $k_c = 18.5$ capping events per filament per second.

The results for the force–velocity relation do not depend on the branching rate as mentioned in the main text. However, the branching rate determines the total number of filaments in the network and therefore also the force which it can carry. Forces in the model are given relative to the constant maximal force f_{fil}^{max} that a filament with orientation $\theta \leq 10^\circ$ is able to carry in its compression mode dominated regime. For the single filament buckling force, by which f_{fil}^{max} could be approximated, a range from 0.5–50 pN has been reported (6). Using an atomic force microscope, it has been measured that an actin network growing against

an obstacle stalls at 150 ± 120 nN for a contact area of about $380 \mu\text{m}^2$ (7), which gives a stall force density of $0.4 \text{ nN}/\mu\text{m}^2$.

In our rate equation approach, we typically have 150 filaments within the branching zone close to the leading edge at intermediate network velocity. For migrating cells, a typical value for the number of filaments per leading-edge length close to the membrane is $90 \pm 10 \mu\text{m}^{-1}$ (3). Dividing by a typical lamellipodium thickness of $3 \mu\text{m}$, we obtain a filament area density of

$30 \mu\text{m}^{-2}$. Comparing with the 150 filaments in our model, we conclude that our model corresponds to a protrusion area of $5 \mu\text{m}^2$. The stall force of $91 f_{\text{fil}}^{\text{max}}$ for the network from simulation then corresponds to the measured value of $0.4 \text{ nN}/\mu\text{m}^2$ for $f_{\text{fil}}^{\text{max}}$ around 22 pN, which lies well inside the reported range (6). This parametrization also implies that the predicted branching rate is 1,482 per second and per μm^2 of leading edge.

1. Maly IV, Borisy GG (2001) Self-organization of a propulsive actin network as an evolutionary process. *Proc Natl Acad Sci USA* 98:11324–11329.
2. Verkhovsky AB, et al. (2003) Orientational order of the lamellipodial actin network as demonstrated in living motile cells. *Mol Biol Cell* 14:4667–4675.
3. Koestler SA, Auinger S, Vinzenz M, Rottner K, Small JV (2008) Differentially oriented populations of actin filaments generated in lamellipodia collaborate in pushing and pausing at the cell front. *Nat Cell Biol* 10:306–313.
4. Peskin CS, Odell GM, Oster GF (1993) Cellular motions and thermal fluctuations: The Brownian ratchet. *Biophys J* 65:316–324.
5. Mogilner A, Oster G (1996) Cell motility driven by actin polymerization. *Biophys J* 71:3030–3045.
6. Chaudhuri O, Parekh SH, Fletcher DA (2007) Reversible stress softening of actin networks. *Nature* 445:295–298.
7. Parekh SH, Chaudhuri O, Theriot JA, Fletcher DA (2005) Loading history determines the velocity of actin-network growth. *Nat Cell Biol* 7:1219–1223.
8. Prass M, Jacobson K, Mogilner A, Radmacher M (2006) Direct measurement of the lamellipodial protrusive force in a migrating cell. *J Cell Biol* 174:767–772.

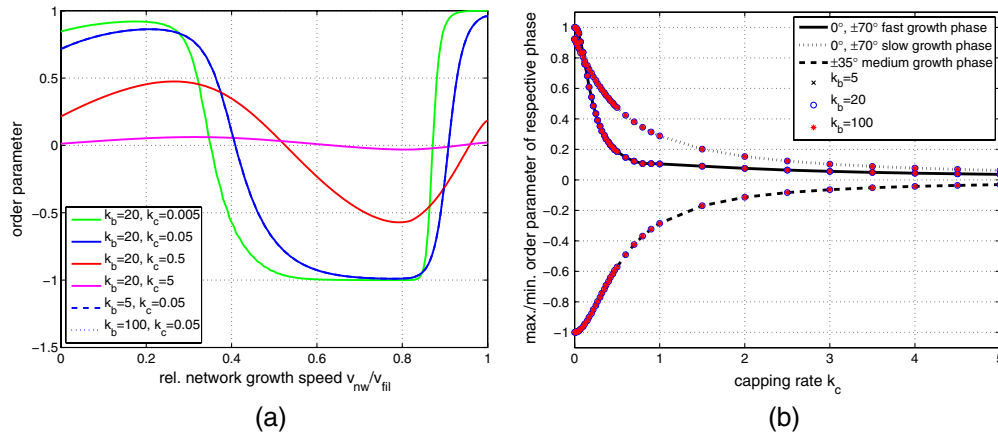


Fig. S1. (A) Order parameter \mathcal{O} as a function of network velocity v_{nw} . The three curves for $k_c = 0.05$ collapse. The order parameter is independent of the choice of the branching rate k_b , whereas for increasing capping rate k_c the differences in the filament orientation patterns diminishes. (B) Peak values of the order parameter \mathcal{O} for the three distinct phases as a function of capping rate k_c . For large capping rates the two different orientation patterns cannot be discriminated well anymore.

